Inorg. Chem. **2002**, *41*, 5675–5685

Inelastic Neutron Scattering on Three Mixed-Valence Dodecanuclear Polyoxovanadate Clusters†

Reto Basler,‡ Grégory Chaboussant,‡ Andreas Sieber,‡ Hanspeter Andres,‡ Mark Murrie,‡ Paul Kögerler,§ Hartmut Bögge,|| Debbie C. Crans,|| Erich Krickemeyer,|| Stefan Janssen,⊥ Hannu Mutka,+ Achim Müller,*,|| and Hans-Ulrich Güdel*,‡

Department of Chemistry and Biochemistry, University of Bern, Freiestrasse 3, 3000 Bern 9, Switzerland, Ames Laboratory, Iowa State University, Ames, Iowa 50011, Faculty of Chemistry, University of Bielefeld, Postfach 100131, 33501 Bielefeld, Germany, Laboratory for Neutron Scattering, PSI & ETHZ, CH-5232 Villigen PSI, Switzerland, and Institute Laue Langevin, Avenue des Martyrs, B. P. 156, F-38042 Grenoble Cedex 9, France

Received March 19, 2002

The magnetic exchange interactions in the mixed-valence dodecanuclear polyoxovanadate compounds $Na_4[V^{IV}_8V^{V}_4As^{III}_8O_{40}(H_2O)]\cdot 23H_2O$, $Na_4[V^{IV}_8V^{V}_4As^{III}_8O_{40}(D_2O)]\cdot 16.5D_2O$, and $(NHEt_3)_4[V^{IV}_8V^{V}_4As^{III}_8O_{40}(H_2O)]\cdot H_2O$ were investigated by an inelastic neutron scattering (INS) study using cold neutrons. In addition, the synthesis procedures and the single-crystal X-ray structures of these compounds have been investigated together with the temperature dependence of their magnetic susceptibilities. The magnetic properties below 100 K can be described by simply taking into account an antiferromagnetically exchange coupled tetramer, consisting of four vanadium(IV) ions. Up to four magnetic transitions between the cluster $S = 0$ ground state and excited states could be observed by INS. The transition energies and the relative INS intensities could be modeled on the basis of the following exchange Hamiltonian: $\hat{H}_{ex} = -2J_{12}^{xy}(\hat{S}_{1x}\hat{S}_{2x} + \hat{S}_{3x}\hat{S}_{4x} + \hat{S}_{1y}\hat{S}_{2y} + \hat{S}_{3y}\hat{S}_{4y}) - 2J_{12}^{z}(\hat{S}_{1z}\hat{S}_{2z} + \hat{S}_{3z}\hat{S}_{4z}) - 2J_{23}^{xy}(\hat{S}_{2x}\hat{S}_{3x} + \hat{S}_{1x}\hat{S}_{4x} + \hat{S}_{2y}\hat{S}_{3y} + \hat{S}_{1y}\hat{S}_{4y}) - 2J_{23}^{z}(\hat{S}_{2z}\hat{S}_{3z} + \hat{S}_{1z}\hat{S}_{4z})$. The following sets of parameters were derived: for $Na_4[V_{12}As_8O_{40}(H_2O)]\cdot 23H_2O$, $J_{12}^{xy} = J_{12}^{z} = -0.80$ meV, $J_{23}^{xy} = J_{23}^{z} = -0.72$ meV; for $Na_4[V_{12}As_8O_{40}(D_2O)]\cdot 16.5D_2O$, $J_{12}^{xy} = J_{12}^{z} = J_{23}^{xy} = J_{23}^{z} = -0.78$ meV; for $(NHEt_3)_4[V_{12}As_8O_{40}(H_2O)]\cdot H_2O$, $J_{12}^{xy} = -0.80$ meV, $J_{12}^{z} = -0.82$ meV, $J_{23}^{xy} = -0.67$ meV, $J_{23}^{z} = -0.69$ meV. This study of the same $\{V_{12}As_8\}$-type cluster in three different crystal environments allows us to draw some conclusions concerning the applicability on INS in the area of nondeuterated molecular spin clusters. In addition, the effects of using nondeuterated samples and different sample container shapes for INS were evaluated.

1. Introduction

Mixed-valence polyoxovanadates(IV/V) represent an intriguing class of high-nuclearity spin cluster anions and display a vast variety of both geometrical and spin structures.[1−3] In certain cases polyoxovanadate cluster anions can even be isolated with different electron populations while their geometry remains virtually identical.[2−4] Mixed-valence polyoxovanadates of the type $\{V^{IV}_xV^{V}_yAs^{III}_8O_{40}(E)\}^{n-}$ (x:y = 6:6, 8:4; E = H_2O, $HCOO^-$) represent an especially interesting subclass displaying spherically shaped cluster geometries, which can encapsulate a formate anion or a water molecule.[5−7] A detailed comparison between the formate- and the water-containing cluster derivatives shows that the introduction of the neutral H_2O guest molecule induces a structural asymmetry; see section 4.1. Here we present

* To whom correspondence should be addressed. E-mail: a.mueller@uni-bielefeld.de, guedel@iac.unibe.ch.

† Dedicated to Professor Gottfried Huttner on occasion of his 65th birthday.

‡ University of Bern.
§ Iowa State University.
|| University of Bielefeld.
⊥ PSI & ETHZ.
+ Institute Laue Langevin.

(1) Müller, A.; Döring, J. *Z. Anorg. Allg. Chem.* **1991**, *595*, 251.
(2) Müller, A.; Sessoli, R.; Krickemeyer, E.; Bögge, H.; Meyer, J.; Gatteschi, D.; Pardi, L.; Westphal, J.; Hovemeier, K.; Rohlfing, R.; Döring, J.; Hellweg, F.; Beugholt, C.; Schmidtmann, M. *Inorg. Chem.* **1997**, *36*, 5239.
(3) Müller, A.; Peters, F.; Pope, M. T. *Chem. Rev.* **1998**, *98*, 239.
(4) Pope, M. T.; Müller, A. *Angew. Chem., Int. Ed. Engl.* **1991**, *30*, 34.
(5) Müller, A.; Döring, J.; Bögge, H. *J. Chem. Soc., Chem. Commun.* **1991**, 273.
(6) Gatteschi, D.; Tsukerblat, B.; Barra, A.-L.; Brunel, L. C.; Müller, A.; Döring, J. *Inorg. Chem.* **1993**, *32*, 2114.
(7) Döring, J. Dissertation, University of Bielefeld, 1990. Here compounds of the type $NaV_{12}H$ and EtV_{12} were described which have a different crystal water content and therefore crystallize in different crystal lattices.

10.1021/ic0202099 CCC: $22.00
Published on Web 10/09/2002

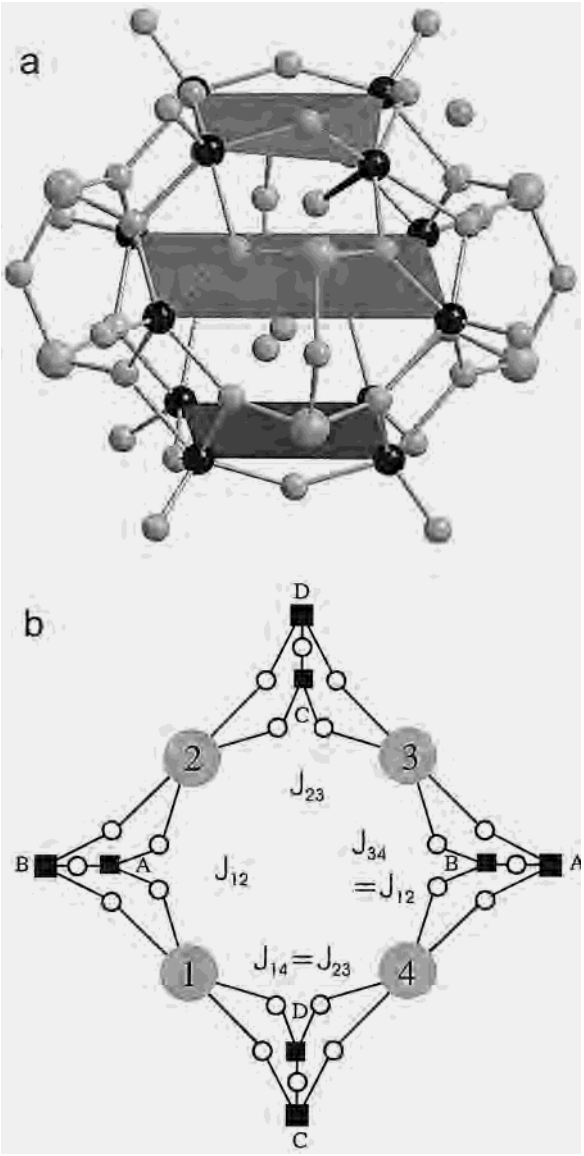

Figure 1. (a) Schematic representation of the $[V_{12}As_8O_{40}(H_2O)]^{4-}$ cluster anion. The three planes formed by the vanadium ions (black spheres) are depicted in dark gray. (b) Schematic view of the central tetramer with definition of the superexchange and parameters pathways through the diarsenite ligands: full squares, As; circles, O.

optimized synthesis methods and detailed investigations on the magnetism of selected compounds of this cluster family, namely $Na_4[V^{IV}{}_8V^{V}{}_4As^{III}{}_8O_{40}(H_2O)]\cdot 23H_2O$ ($NaV_{12}H$), $Na_4[V^{IV}{}_8V^{V}{}_4As^{III}{}_8O_{40}(D_2O)]\cdot 16.5D_2O$ ($NaV_{12}D$), and $(NHEt_3)_4[V^{IV}{}_8V^{V}{}_4As^{III}{}_8O_{40}(H_2O)]\cdot H_2O$ (EtV_{12}). The structure of their $\{V_{12}As_8\}$-type anions (of approximate D_{4h} symmetry) can be derived from an O_{24} rhombicuboctahedron, the 18 O_4 squares of which are capped by 12 VO and 4 As_2O groups. This results in a stack of three V_4 squares which are bridged via diarsenite ($As_2O_5^{4-}$) groups, sketched in Figure 1a. Bond valence sum (BVS) calculations show that four of the eight V(3d) electrons are localized in the central V_4 square (V$\cdot\cdot\cdot$V = 5.26−5.31 Å). The 2 + 2 remaining V(3d) electrons are delocalized over the two outer V_4 squares (V$\cdots$V = 3.41−3.45 Å). This electronic configuration of the outer squares was shown to give rise to a large singlet−triplet splitting with the singlet lying lowest.[5,6] The low-temperature magnetic properties were therefore interpreted to result from the exchange interactions in the inner square.

Although this model is very plausible from a chemical point of view, the observed magnetic susceptibility data could also be interpreted with other coupling schemes. We therefore decided to study three different compounds containing the $\{V_{12}As_8\}$-type cluster in slightly different geometries by a combination of magnetic susceptibility measurements and inelastic neutron scattering (INS). INS has proven to be a very powerful tool in the study of exchange and anisotropy interactions in polynuclear complexes of transition metal and lanthanide ions.[8−11] As a spectroscopic technique it provides direct access to the energy splittings in the ground state. Thus, in contrast to bulk techniques such as magnetic or calorimetric measurements, no theoretical model is required to derive the exchange and anisotropy splittings. Compared to high-field EPR, which is very powerful in spin cluster research,[12,13] INS has the additional advantage that no external magnetic field is required. Depending on the neutron wavelength chosen, magnetic excitations up to about 12 meV (cold neutrons) or about 50 meV (thermal neutrons) can be measured. A disadvantage of neutron scattering in the study of molecular magnetic compounds and molecular spin clusters, in particular, lies in the huge incoherent scattering cross section of H atoms. Thus for most applications at least partial deuteration is mandatory. This, on the other hand, is a very severe restriction in spin cluster research, because deuteration of such species is often prohibitive. Nonetheless it was recently shown that magnetic excitations of undeuterated spin clusters can be studied in a limited energy range.[14,15]

Our objective in this study was thus 2-fold: The energy splittings resulting from exchange interactions were to be determined directly by INS. We tested whether the parameters given in refs 6 and 16 are adequate to account for these splittings. Since we had both deuterated and nondeuterated compounds containing the $[V_{12}As_8O_{40}(H_2O)]^{4-}$ anion, we were interested to investigate what limitations were imposed by the presence of H atoms in our INS study.

2. Experimental Section

2.1. General Methods. Chemicals were purchased from Merck, Alfa Aesar, and Fluka. IR spectra were acquired using a Bruker IFS66, and UV−vis spectra were measured using a Shimadzu UV-160A. In addition, magnetic susceptibility data were obtained using a Quantum Design MPMS-XL magnetometer.

(8) Güdel, H. U.; Furrer, A. *Mol. Phys.* **1977**, *33*, 1335.
(9) Furrer, A.; Güdel, H. U.; Blank, H.; Heidmann, A. *Phys. Rev. Lett.* **1989**, *62*, 210.
(10) Andres, H.; Clemente-Juan, J. M.; Aebersold, M.; Güdel, H. U.; Coronado, E.; Büttner, H.; Kearly, G.; Melero, J.; Burriel, R. *J. Am. Chem. Soc.* **1999**, *121*, 10028.
(11) Mirebeau, I.; Hennion, M.; Casalta, H.; Andres, H.; Güdel, H. U.; Irodova, A. V.; Caneschi, A. *Phys. Rev. Lett.* **1999**, *83* (3), 628.
(12) Barra, A.-L.; Brunel, L.-C.; Gatteschi, D.; Pardi, L.; Sessoli, R. *Acc. Chem. Res.* **1998**, *31*, 460.
(13) Barra, A.-L.; Gatteschi, D.; Sessoli, R. *Phys. Rev. B* **1997**, *56*, 8192.
(14) Caciuffo, R.; Amoretti, G.; Murani, A.; Sessoli, R.; Caneschi, A.; Gatteschi, *D. Phys. Rev. Lett.* **1998**, *81* (21), 4744.
(15) Andres, H.-P.; Basler, R.; Güdel, H. U.; Aromí, G.; Christou, G.; Büttner, H.; Rufflé, B. *J. Am. Chem. Soc.* **2000**, *122* (50), 12469.

2.2. Synthesis of $Na_4[V^{IV}_8V^{V}_4As_8O_{40}(H_2O)]\cdot 23H_2O$. In a 100-mL wide necked Erlenmeyer flask (covered by a watch glass), 2.93 g (24.0 mmol) of $NaVO_3$ and 1.58 g (8.00 mmol) of As_2O_3 doubly sublimed are successively dissolved in 75 mL of N_2-saturated water at 90 °C. After cooling of the clear yellow solution to 80 °C, 0.493 g (3.75 mmol) of $N_2H_4\cdot H_2SO_4$ is slowly added and the solution is stirred for 30 min. The solution is left for 2 h without stirring (covered by a watch glass) at 80 °C. After being cooled to room temperature, the green solution is left standing for 16 h without stirring. A small amount of a colorless precipitate is then filtered off, and the pH value of the filtrate is adjusted to 6.0 using ca. 5 mL of 1 M HCl solution (a green precipitate is formed while adjusting the pH value which is quickly redissolved upon stirring). The pH has to be readjusted to 6.0 after ca. 30 min. The solution is then stored in a closed flask at 4 °C. After 2−3 days, precipitated dark blue crystals are filtered off, washed with 2-propanol, dried in an argon stream, and stored under argon atmosphere. Yield: 2.5 g (53% based on V).

2.3. Synthesis of $Na_4[V^{IV}_8V^{V}_4As_8O_{40}(D_2O)]\cdot 16.5D_2O$. The deuterated derivative was prepared according to the method previously described in a thesis,[7] but D_2O and 33% DCl solution were used instead of H_2O and 1 M HCl solution.

The method of synthesis is crucial in determining the solvent molecule content of the sodium salts of the $\{V_{12}As_8\}$-type cluster anions and thus also for the crystal structure of the two modifications. The two sodium salts $Na_4V_{12}H$ and $Na_4V_{12}D$ used in this study were prepared differently and thus had different solvent contents and thus different crystal structures.

2.4. Synthesis of $(NH(C_2H_5)_3)_4[V^{IV}_8V^{V}_4As_8O_{40}(H_2O)]\cdot H_2O$. In a 100-mL wide-necked Erlenmeyer flask (covered by a watch glass), 2.93 g (24.0 mmol) of $NaVO_3$, 1.58 g (8.00 mmol) of As_2O_3 doubly sublimed, and 1.50 g (10.9 mmol) of $NH(C_2H_5)_3Cl$ are successively dissolved in 50 mL of N_2-saturated water at 90 °C. After cooling of the clear yellow solution to 80 °C, 205 mg (3 mmol) of $N_2H_4\cdot$HCl is slowly added. The solution is left for 2 h without stirring (covered by a watch glass) at 80 °C. After being cooled to room temperature, the green solution is left standing for 16 h without stirring. A small amount of a colorless precipitate is then filtered off, and the pH value of the filtrate is adjusted to 6.0 using ca. 5 mL of 1 M HCl (a green precipitate is formed while adjusting the pH value which is quickly redissolved upon stirring). The resulting solution is stored in a closed flask at room temperature for crystallization. Dark blue rhombohedral crystals of $(NHEt_3)_4[V^{IV}_8V^{V}_4As_8O_{40}(H_2O)]\cdot H_2O$ are formed after 2−3 days and are filtered off, washed with ice cold water, and dried over $CaCl_2$ in a desiccator under an argon atmosphere. Yield: 1.9 g (29% based on V). If the compound is prepared according to the method described in a thesis,[7] dark green needle-shaped crystals containing a $\{V_{14}As_8\}$-type cluster compound as described in ref 1 are formed as a byproduct.

2.5. X-ray Crystallography. Crystals were taken from the mother liquor and mounted on a glass fiber. Diffraction data were collected on a Bruker AXS three-circle diffractometer with a 1K-CCD detector. The cell parameters were obtained from a least-squares fit to the angular coordinates of all reflections. Intensities were integrated from a series of frames (0.3° ω-rotation) covering more than a hemisphere of reciprocal space. A total of 26 821 and 24 331 reflections for $(NHEt_3)_4[V_{12}As_8O_{40}(H_2O)]\cdot H_2O$ and $Na_4[V_{12}As_8O_{40}(H_2O)]\cdot 23H_2O$ were collected, respectively. The data were merged to provide a data set containing 9567 and 8793 unique reflections ($R_{int} = 0.0209$ and $R_{int} = 0.0213$). The structures were solved by direct methods (using SHELXS-97) and refined (with SHELXL-93 on F^2 using all data) by a full-matrix, weighted least-squares process to the residuals given in Table 1. All non-hydrogen atoms (not disordered) were refined by using anisotropic displacement parameters. For the compound $(NHEt_3)_4[V_{12}As_8O_{40}(H_2O)]\cdot H_2O$ two O═V−OH_2 groups are found to be disordered whereas $Na_4[V_{12}As_8O_{40}(H_2O)]\cdot 23H_2O$ displays eight such disordered groups. Given the smaller structural uncertainty, we provide more details for the compound $(NHEt_3)_4[V_{12}As_8O_{40}(H_2O)]\cdot H_2O$. The occupancy factors for the disordered positions were refined to sort out the disorder and the bond distances. For the compound $(NHEt_3)_4[V_{12}As_8O_{40}(H_2O)]\cdot H_2O$ the occupancy factors for the two disordered sites were 0.5, and as described in the Results and Discussion, these two sites cannot be occupied independently. The assignments of oxidation states to the vanadium positions were based on bond valence sum calculations. Details regarding the crystallographic experiment and computations for compounds $(NHEt_3)_4[V_{12}As_8O_{40}(H_2O)]\cdot H_2O$ and $Na_4[V_{12}As_8O_{40}(H_2O)]\cdot 23H_2O$, respectively, are listed in Table 1. Selected bond lengths and bond angles are given in the Supporting Information. Further details on the crystal structure investigation of $Na_4[V_{12}As_8O_{40}(H_2O)]\cdot 23H_2O$ may be obtained from the Fachinformationszentrum Karlsruhe, D-76344 Eggenstein-Leopoldshafen, Germany (fax (++49) 7247-808-666; E-mail crysdata@fiz-karlsruhe.de), on quoting the depository number CSD 412387. Crystallographic data (excluding structure factors) for $(NHEt_3)_4[V_{12}As_8O_{40}(H_2O)]\cdot H_2O$ have been deposited with the Cambridge Crystallographic Data Centre as supplementary publication no. CCDC-179691. Copies of the data can be obtained free of charge on application to CCDC, 12 Union Road, Cambridge CB2 1EZ, U.K. (fax (+44) 1223-336-033; E-mail deposit@ccdc.cam.ac.uk).

Table 1. Crystallographic Data for the Compounds $(NHEt_3)_4[V_{12}As_8O_{40}(H_2O)]\cdot H_2O$ and $Na_4[V_{12}As_8O_{40}(H_2O)]\cdot 23H_2O$

	$Na_4[V_{12}As_8O_{40}(H_2O)]\cdot 23H_2O$	$(NHEt_3)_4[V_{12}As_8O_{40}(H_2O)]\cdot H_2O$
empirical formula	$H_{48}As_8Na_4O_{64}V_{12}$	$C_{24}H_{68}As_8N_4O_{42}V_{12}$
cryst dimens (mm)	0.16 × 0.16 × 0.12	0.40 × 0.30 × 0.15
space group	$P2_1/c$	$P2_1/n$
a (pm)	1340.46(4)	1215.90(3)
b (pm)	1146.90(3)	2122.99(6)
c (pm)	1973.72(6)	1370.63(4)
β (deg)	95.744(1)	111.778(1)
V (10^6 pm^3)	3019.1(2)	3285.5(2)
Z	2	2
D_{calc} (g/cm^3)	2.613	2.320
μ(Mo Kα) (mm^{-1})	6.276	5.717
T (K)	183(2)	183(2)
final R indices [$I > 2\sigma(I)$][a]	R1 = 0.0295, wR2 = 0.0820	R1 = 0.0265, wR2 = 0.0618

[a] $R1 = \Sigma||F_o| - |F_c||/\Sigma|F_o|$; $wR2 = [\Sigma w(F_o^2 - F_c^2)^2/\Sigma w(F_o^2)^2]^{1/2}$; $1/w = [\sigma^2(F_o^2) + (0.05P)^2 + 4P]$ for $Na_4[V_{12}As_8O_{40}(H_2O)]\cdot 23H_2O$; $1/w = [\sigma^2(F_o^2) + (0.03P)^2 + 2P]$ for $(NHEt_3)_4[V_{12}As_8O_{40}(H_2O)]\cdot H_2O$; $P = (F_o^2 + 2F_c^2)/3$.

2.6. Characterization. All compounds were characterized by infrared spectroscopy, magnetic susceptibility, and especially powder X-ray diffraction. Theoretical powder X-ray diffraction patterns were calculated using the program WinXPow on the basis of the single-crystal X-ray data. For $(NHEt_3)_4[V_{12}As_8O_{40}(H_2O)]\cdot H_2O$ (EtV_{12}) calculated and measured X-ray patterns agreed. The same was true for the deuterated version of $Na_4[V_{12}As_8O_{40}(H_2O)]\cdot 16.5H_2O$ ($NaV_{12}D$). For $Na_4[V_{12}As_8O_{40}(H_2O)]\cdot 23H_2O$ ($NaV_{12}H$) it was not possible to characterize the phase of the polycrystalline compound using powder X-ray diffraction, since it seems to lose solvent molecules upon grinding and therefore changes its structure. Thus, we used single-crystal X-ray diffraction analysis of a crystal taken out from the same batch, which was later used for our INS studies, to specify its modification. This crystal showed the expected

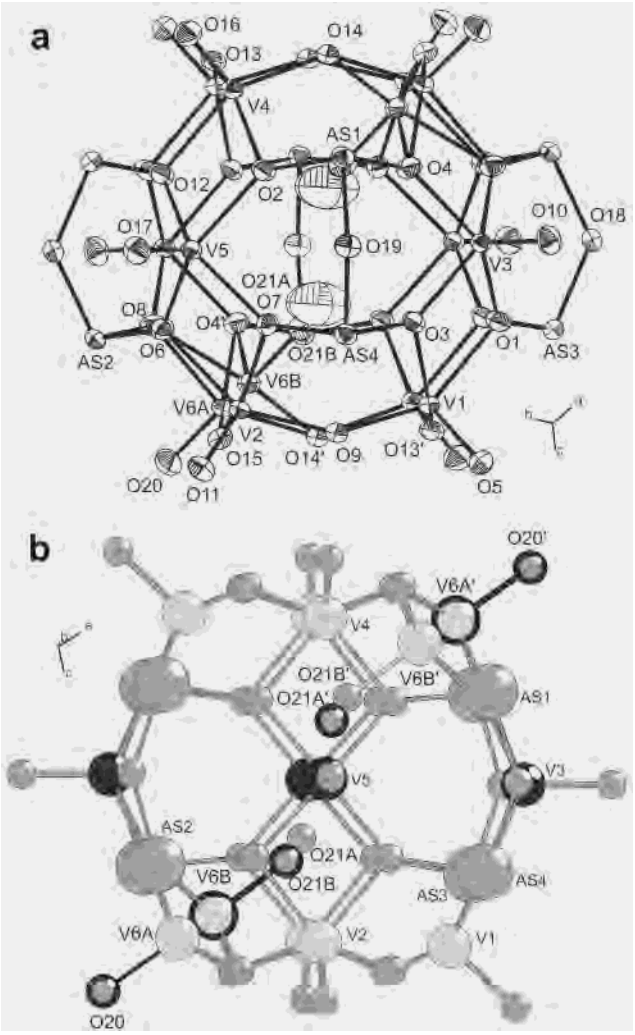

Figure 2. (a) Structure of the $[V^{IV}_8V^{V}_4As_8O_{40}(H_2O)]^{4-}$ cluster in $(NHEt_3)_4[V_8V_4As_8O_{40}(H_2O)]\cdot H_2O$. Thermal ellipsoids and the atomic labeling scheme are shown. Both sites for the disordered positions are shown (V6A/V6B and V6A′/V6B′). This view emphasizes the As_2O groups of the cluster. (b) Same anion is shown in a different view focusing on the octahedrally coordinated V6 atom (V6B′, lower left). The mixed-valent V(IV)/V(V) centers are shown as medium-sized gray circles; the V(IV) atoms are shown in black. The As positions are represented by large gray circles, and the oxygen positions, by small gray circles. This orientation illustrates the disorder problem found for this cluster.

characteristics of the $Na_4[V_{12}As_8O_{40}(H_2O)]\cdot 23H_2O$ modification. In addition, the magnetic susceptibility versus temperature curves were similar for all three samples; see section 3. There is no doubt, therefore, that the $[V_{12}As_8O_{40}(H_2O)]^{4-}$ cluster type anion is present in all three samples. Slight differences in the cluster geometry, as determined by single-crystal X-ray crystallography, will be used to interpret the slight differences in the exchange splittings.

For EtV_{12} we used two different container shapes for the INS experiments. Either approximately 3 g of the blue crystalline sample of EtV_{12} was sealed under helium into a 2 mm thick aluminium slab shaped container with a sample area of 29 × 39 mm^2 or approximately 6 g was sealed under helium into an aluminium container of cylindrical shape of 15 mm in diameter and 50 mm length. About 1.5 g of sample $NaV_{12}H$ was sealed under helium into a slab container having the dimensions 27 × 47 × 2 mm's. For sample $NaV_{12}D$ we used approximately 6 g of a blue polycrystalline sample sealed under helium in a cylindrical aluminium container having the same dimensions as described above.

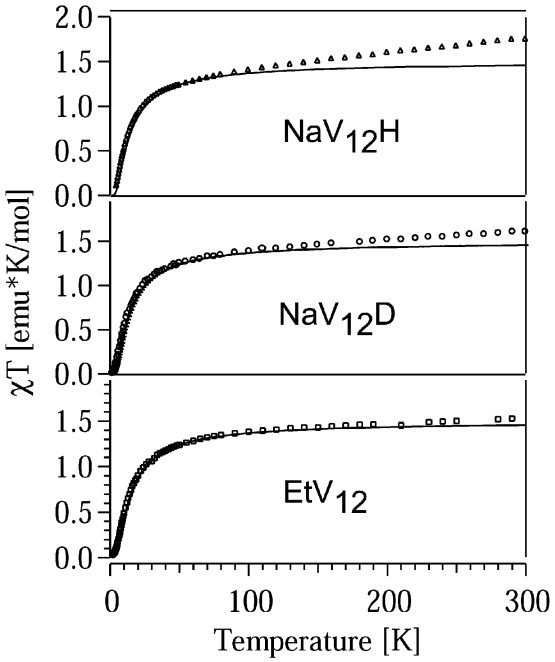

Figure 3. Measured magnetic susceptibility of polycrystalline samples of $NaV_{12}H$, $NaV_{12}D$, and EtV_{12} between 1.8 and 300 K. The solid lines represent the calculated susceptibility when applying the Hamiltonian in eq 4 supplemented by an appropriate Zeeman term and the parameters given in Table 5. An isotropic g value of $g = 1.97$ was adopted from ref 6.

INS spectra were recorded on the time-of-flight instruments IN4 (thermal neutrons) and IN6 (cold neutrons) at the ILL (Grenoble, France) and on FOCUS (cold neutrons) at the PSI (Villigen, Switzerland) using either neutrons of $\lambda = 1.1$ Å (IN4) and 4.1 and 5.9 Å (IN6) between 1.8 and 30 K at the ILL or using neutrons of $\lambda = 2.29$ Å at 1.5, 30, and 100 K at the PSI. The data treatment involved the subtraction of a spectrum of an empty aluminium container of the same size and the calibration of the detectors by means of a spectrum of vanadium metal. The time-of-flight to energy conversion and the data reduction were done using the standard programs INX at the ILL and NINX at the PSI. Further data treatment was done using the commercial program Igor-Pro 3.14 (Wavemetrics).

Susceptibility measurements were carried out in the range 300−1.8 K in a field of 0.1 T using a Quantum Design MPMS-XL SQUID magnetometer.

3. Results

The $[V^{IV}_8V^{V}_4As_8O_{40}(H_2O)]^{4-}$ cluster structure in crystals of EtV_{12} is depicted in Figure 2; the crystallographic details are given in Table 1, and bond lengths and bond angles, in the Supporting Information. Figure 3 shows the experimental χT data for $NaV_{12}H$, $NaV_{12}D$, and EtV_{12} as a function of temperature in the range of 1.8−300 K. Below 100 K the data are practically coincident for the three samples. Between 100 and 300 K there are slight differences.

Figure 4 shows energy-loss INS data in the energy transfer range 0 to 60 meV of $NaV_{12}D$ measured at 1.1 Å on IN4 at 1.5 K for several values of the elastic scattering vector Q. The inelastic peaks centered at 29.3, 34.6, 48.1, and around 10 meV clearly show increasing intensity with increasing Q values. Figure 5 shows energy-loss spectra at 1.5 K in the range 0−13 meV of $NaV_{12}H$, $NaV_{12}D$, and EtV_{12} obtained

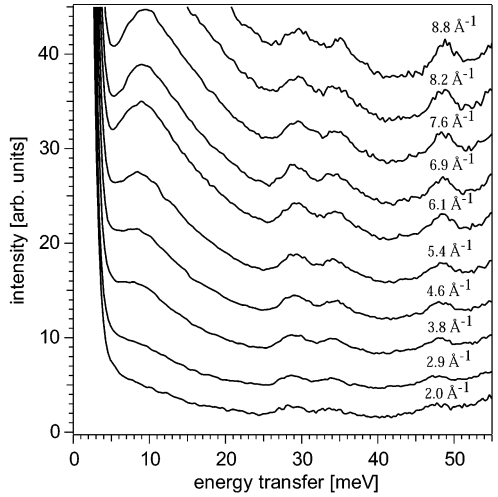

Figure 4. Energy-loss INS spectra of $NaV_{12}D$ at 1.5 K measured on IN4 with $\lambda = 1.1$ Å for various values of the elastic scattering vector Q.

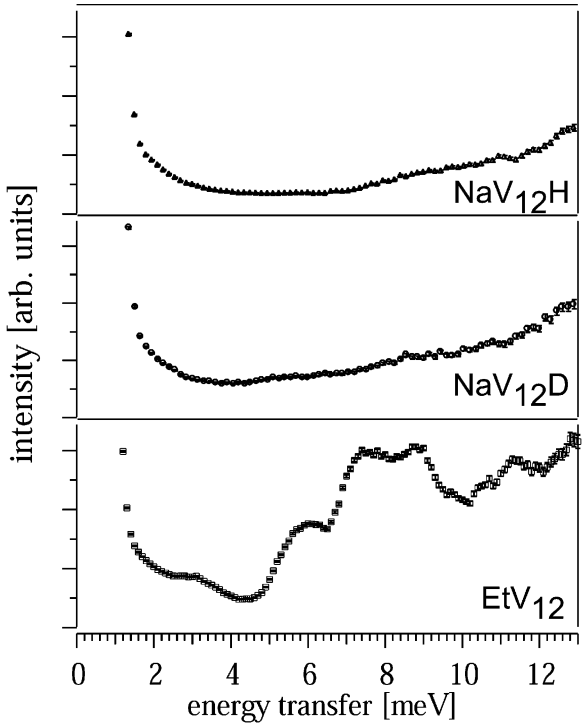

Figure 5. INS spectra of $NaV_{12}H$, $NaV_{12}D$, and EtV_{12} (cylinder) recorded on FOCUS with an incident neutron wavelength of 2.29 Å at a temperature of 1.5 K in the range 0−13 meV, covering the Q range from 0.5 to 5.0 Å^{-1}. The y axis of the spectra has been normalized at the elastic line so that they are comparable.

with $\lambda = 2.29$ Å on FOCUS. The spectra are normalized with respect to the integrated intensity of the elastic line. We note that both the $NaV_{12}H$ and EtV_{12} spectra do not have a significantly enhanced background due to incoherent scattering, usually seen in hydrogen atom containing materials. This is a result of the thin slab container used for these samples, in contrast to the cylindrical container for $NaV_{12}D$. The obvious difference between the EtV_{12} and the Na samples are the pronounced inelastic features between 5 and 12 meV in EtV_{12}, which are completely absent in the other two spectra. Figure 6 shows energy-loss INS spectra of the three compounds in the range −3.5 to +3.5 meV obtained

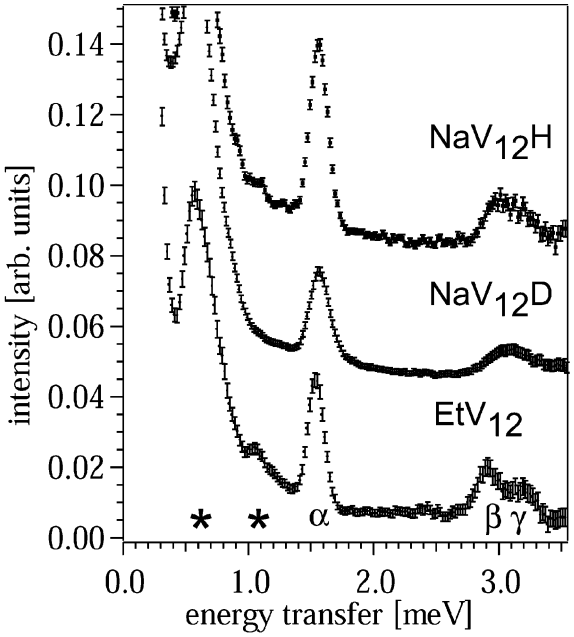

Figure 6. INS spectra of $NaV_{12}H$, $NaV_{12}D$, and EtV_{12} (slab) at 1.9 K recorded on IN6 with an incident neutron wavelength of $\lambda_i = 4.1$ Å in the energy-transfer range 0−3.6 meV, covering the Q range from 0.27−2.6 Å^{-1}. The spectra have been normalized with respect to the intensity of the elastic lines. The bands marked by asterisks are instrumental artifacts, also seen in the empty can runs.

at 1.9 K with a wavelength of 4.1 Å and thus with a significantly better instrumental resolution than in Figures 4 and 5. The features indicated with asterisks in Figure 6 are experimental artifacts, also seen in the empty can runs. Around 1.5 meV we observe the well-defined inelastic peak α and at around 3 meV the partially resolved peaks β and γ in all the three samples. The energies of the peaks α, β, and γ for all three compounds are collected in Table 3.

Figure 7 shows INS spectra of EtV_{12} with the same neutron wavelength and spectral resolution as in Figure 6 for five temperatures between 1.9 and 37.7 K. The spectra have been analyzed by subtracting a background and fitting the inelastic features with least-squares Gaussians. Both the energy loss and energy gain sides are shown. The α, β, and γ bands on the loss side decrease in intensity with increasing temperature, whereas their counterparts α′, β', and γ' on the neutron energy gain side are growing with increasing temperature. As EtV_{12} is warmed above 10 K, β and γ are no longer resolved, instead a single peak emerges at the mean value of β and γ. At the same time, the sharp peak at α loses intensity and broadens substantially consistent with theemergence of a pair of peaks δ at 1.3 meV and ϵ at 1.7 meV. As will be shown in the discussion, sections 4.2 and 4.3, this splitting and temperature dependence is reproduced by the model required to explain the splitting between β and γ. The energies and relative intensities of the energy-loss features in the spectra of Figure 7 are collected in Table 4.

Figure 8 shows INS energy-loss spectra at 1.9 K in the energy range of 1.2−1.55 meV of all three compounds measured with a neutron wavelength of 5.9 Å and correspondingly better instrumental resolution in the region of the α band. The α band is clearly split into two components

Table 2. Selected Bond Lengths (Å) and Angles (deg) for $(NHEt_3)_4[V_{12}As_8O_{40}(H_2O)]\cdot H_2O$

As(1)−O(4)	1.763(2)	V(6A)−O(8)	2.049(2)
As(1)−O(2)	1.772(2)	V(6A)−O(4)′	2.051(2)
As(1)−O(19)	1.793(2)	V(6A)−O(21B)	2.404(5)
V(1)−O(5)	1.623(2)	V(6B)−O(21B)	1.633(5)
V(1)−O(13)′	1.795(2)	V(6B)−O(15)	1.752(2)
V(1)−O(9)	1.796(2)	V(6B)−O(14)′	1.791(2)
V(1)−O(3)	2.043(2)	V(6B)−O(8)	2.059(2)
V(1)−O(1)	2.050(2)	V(6B)−O(4)′	2.068(2)
		V(6B)−O(21A)	2.120(10)
V(6A)−V(6B)	0.772(1)	V(6B)−O(20)	2.410(2)
V(6A)−O(20)	1.638(2)		
V(6A)−O(15)	1.832(2)	O(21A)−O(21B)	0.520(10)
V(6A)−O(14)′	1.862(2)		

O(4)−As(1)−O(2)	98.41(8)	O(15)−V(6A)−O(4)′	148.23(8)
O(4)−As(1)−O(19)	99.25(7)	O(14)′−V(6A)−O(4)′	87.61(7)
O(2)−As(1)−O(19)	98.52(7)	O(8)−V(6A)−O(4)′	72.02(7)
O(5)−V(1)−O(13)′	106.32(8)	V(6B)−V(6A)−O(20)	177.7(1)
O(5)−V(1)−O(9)	105.71(8)		
O(13)′−V(1)−O(9)	98.17(7)	O(21B)−V(6B)−O(15)	99.3(2)
O(5)−V(1)−O(3)	104.36(8)	O(21B)−V(6B)−O(14)′	98.8(2)
O(13)′−V(1)−O(3)	146.01(7)	O(15)−V(6B)−O(14)′	104.12(8)
O(9)−V(1)−O(3)	87.24(7)	O(21B)−V(6B)−O(8)	98.9(2)
O(5)−V(1)−O(1)	104.34(8)	O(15)−V(6B)−O(8)	89.77(7)
O(13)′−V(1)−O(1)	86.33(7)	O(14)′−V(6B)−O(8)	155.38(8)
O(9)−V(1)−O(1)	146.92(7)	O(21B)−V(6B)−O(4)′	98.7(2)
O(3)−V(1)−O(1)	72.12(6)	O(15)−V(6B)−O(4)′	155.76(8)
O(20)−V(6A)−O(15)	106.90(9)	O(14)′−V(6B)−O(4)′	88.99(7)
O(20)−V(6A)−O(14)′	105.78(9)	O(8)−V(6B)−O(4)′	71.49(7)
O(15)−V(6A)−O(14)′	98.31(8)	O(21B)−V(6B)−O(20)	177.7(2)
O(20)−V(6A)−O(8)	102.07(9)	O(15)−V(6B)−O(20)	82.56(8)
O(15)−V(6A)−O(8)	87.88(7)	O(14)′−V(6B)−O(20)	81.96(7)
O(14)′−V(6A)−O(8)	148.20(8)	O(8)−V(6B)−O(20)	79.79(7)
O(20)−V(6A)−O(4)′	101.33(9)	O(4)′−V(6B)−O(20)	79.16(7)

[a] Symmetry transformations used to generate equivalent atoms (marked with a prime): $-x, -y, -z$.

Table 3. Experimental and Calculated Transition Energies α, β, and γ Using Eq 4 and the Parameters Given in Table 5 for Compounds $NaV_{12}H$, $NaV_{12}D$, and EtV_{12} with Experimental Errors in Parentheses

	energy (meV)					
	$NaV_{12}H$		$NaV_{12}D$		EtV_{12}	
transition	expt	calcd	expt	calcd	expt	calcd
α	1.55(1)	1.53	1.57(1)	1.56	1.54(1)	1.50
β	2.98(8)	2.97	3.08(1)	3.12	2.90(1)	2.85
γ	3.2(1)	3.1			3.18(1)	3.11

α_1 and α_2 in EtV_{12}, whereas in $NaV_{12}D$ and $NaV_{12}H$ there is no evidence for a splitting but the band is significantly broadened. In EtV_{12} this spectral region was measured as a function of temperature. The energies and relative intensities of α_1 and α_2 are separately listed for the lowest two temperatures in Table 4.

On the basis of the experimental INS data presented in Figures 5−7 and Tables 3 and 4, we derive the empirical energy-level diagrams shown in Figure 9 for the three compounds.

A comparison of the influence of different container shapes on the measured *Q*-dependence of INS transitions is shown in Figure 10 for EtV_{12}. The 1.9 K data in Figure 10a,b correspond to cylindrical and slab containers, respectively. The intensities of α, β, and γ are given as a function of the scattering vector *Q*.

4. Analysis and Discussion

4.1. Structural Description of the $[V_{12}As_8O_{40}(H_2O)]^{4-}$ Anion in $(NHEt_3)_4[V_{12}As_8O_{40}(H_2O)]\cdot H_2O$. As the structures of the anions in $(NHEt_3)_4[V_{12}As_8O_{40}(H_2O)]\cdot H_2O$ and $Na_4[V_{12}As_8O_{40}(H_2O)]\cdot 23H_2O$ are virtually identical and crystals of $Na_4[V_{12}As_8O_{40}(H_2O)]\cdot 23H_2O$ display a higher degree of structural disorder, the following discussion is focused on the compound $(NHEt_3)_4[V_{12}As_8O_{40}(H_2O)]\cdot H_2O$. The structure of the cluster anion $[V_{12}As_8O_{40}(H_2O)]^{4-}$ is closely related to the previously reported $\{V_{12}As_8\}$-type cluster anion encapsulating a formate ion[5] but displays in the EtV_{12} and NaV_{12} salts a structural asymmetry caused by one octahedrally coordinated V center. We refer in the following to Figure 2a,b. The spherical polyoxometalate cluster consists of 11 square pyramidally coordinated V centers (V1, V2, V3, V4, V5, their symmetrical counterparts, and V6A), 1 octahedrally coordinated V center (V6B), 8 As centers, and 40 oxygen centers. The oxidation states of the V positions are determined by analysis of the BVS. According to this, the four equatorial V (V3, V5, and their symmetrical counterparts) centers forming the central V_4 square, each bound to two $O_2As-O-AsO_2$ bridges, are in the oxidation state +4, while the remaining V centers show an intermediate oxidation state of +4.5. Due to one octahedrally coordinated V center (V6B), the symmetry of the structure is decreased: as shown in Figure 2a, the positions V6 and O21 both are disordered in the crystal lattice and are each found on two positions with equal occupancy factors (V6A/V6B and O21A/O21B, respectively). The corresponding symmetry related positions are marked with a apostrophe in Figure 2b. A close inspection of the interatomic distances shows that the following pairs of positions cannot be occupied in the same anion due to too short distances between positions O21A/O21B (0.52 Å) and O21A/O21A′ (2.21 Å). We illustrate this in Figure 2b by highlighting the atoms likely to be occupied in a given cluster. Thus, this arrangement can be described to consist of one V=O group (V6A′−O20 = 1.64 Å) as a part of a "usual" VO_5 square pyramid, one uncoordinated H_2O molecule (O21A′), and one O=V−OH_2 group (V6B−O21B = 1.63 Å, B6B−O20 = 2.41 Å) as a part of a VO_6 octahedron. The calculated bond valence sum value for the V atom of the VO_6 octahedron amounts to 4.8, suggesting a greater V(V) character, but BVS values calculated from such disordered positions always bear considerable uncertainties. Correspondingly, the remaining vanadium positions of the outer V_4 squares display slightly decreased BVS values compared to those found for the related formate encapsulated cluster. The asymmetry in the cluster can be attributed to the size of the cavity which is too large to accommodate only one H_2O molecule but is not sufficiently large to enclose two H_2O molecules. However, the space inside the cluster sphere allows the encapsulated water molecule (e.g. H_2O21A′) to form hydrogen bonds to an inward oriented O−V (e.g. O21B−V6B) group. The observed distance between the O center of the H_2O molecule and the O position of the neighboring O−V group is 2.67 Å, a nearly optimal value for hydrogen bonds. The asym-

Table 4. Experimental and Calculated Energies and Relative Intensities of the INS Transitions of $(NHEt_3)_4[V_{12}As_8O_{40}]\cdot H_2O$ at Incident Neutron Wavelengths of $\lambda_i = 5.9$ Å and 4.1 Å[a]

			normalized intensity energy loss							
	energy (meV)		1.9 K		5.4 K		10.3 K		19.1 K	
Label	Expt	calcd	expt	calcd	expt	calcd	expt	calcd	expt	calcd
α_1 } α	1.45(1)	1.4 7	1.00(7)	1.0 0	0.89(7)	0.88	0.82(5)[c]	1.76[c]	0.59(4)[c]	0.89[c]
α_2 }	1.51(1)	1.51	1.88(8)	2.27	1.77(8)	2.01				
β	2.90(1)	2.85	1.12(5)	1.13						
γ	3.18(1)	3.11	0.69(4)	0.67	1.76(1)[b]	1.73[b]	1.43(7)[b]	1.38[b]	1.2(1)[b]	0.88[b]
φ	3.1(1)	3.0								
δ	1.4(1)	1.4			0.07(3)	0.10	0.14(1)	0.35	0.26(3)	0.47
ϵ	1.7(1)	1.6				0.10	0.11(3)	0.37	0.19(3)	0.50

[a] The intensities were scaled to a value of 1.0 for transition α_1 at 1.9 K. The theoretical energies were calculated using eq 4 with the parameters given in Table 5. The intensities were calculated using eq 5 and the program MAGPACK.[17] [b] β, γ, and φ could not be resolved completely. [c] α_1 and α_2 could not be resolved completely.

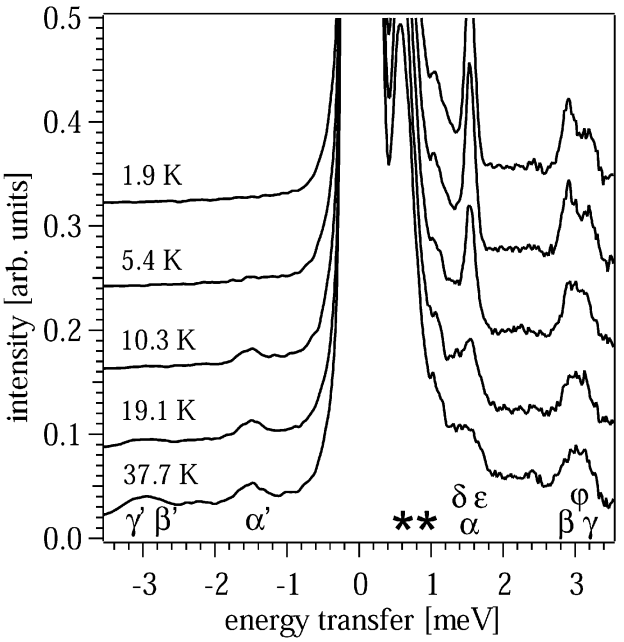

Figure 7. INS spectra of EtV_{12} measured in a slab recorded on IN6 at $\lambda_i = 4.1$ Å for various temperatures. The peaks are labeled at the bottom of the figure.

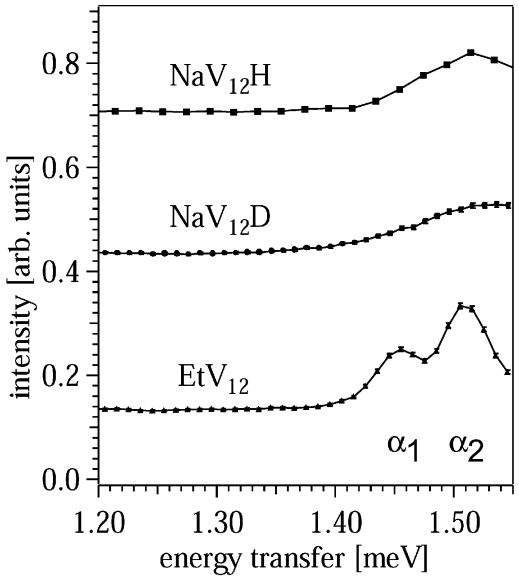

Figure 8. INS spectra of $NaV_{12}H$, $NaV_{12}D$, and EtV_{12} (cylinder) collected on IN6 with an incident neutron wavelength of $\lambda_i = 5.9$ Å covering the Q range from 0.19 to 1.79 $Å^{-1}$. The lines are drawn to guide the eyes.

metry of this anion can therefore be assumed to result from a displacement of one O−V group toward the center of the cluster sphere to interact with the water molecule. As a result of this perturbation, a second water molecule coordinates trans-positioned to the inward oriented O−V group, completing the octahedral coordination sphere of the corresponding vanadium center of this O−V group. In Figure 2a all the atoms are shown, although only one set of the groups V6A(−O20)/V6B(−O20) and V6A′ (−O20′)/V6B′(−O20′) can be occupied at one time. In Figure 2b this is illustrated by highlighting one set of these groups. The octahedral V center (V6B) is shown at the bottom left; when this group is occupied, the V6A−O20 group is not occupied and vice versa.

4.2. Exchange Coupling and INS Cross Section. The magnetic susceptibility of the isoelectronic and structurally closely related cluster $[V_{12}As_8O_{40}(HCO_2)]^{5-}$ was reported in refs 5 and 6. These were supplemented by EPR data in ref 6. For the analysis[16] it was assumed that each of the smaller dark squares in Figure 1 contains two V^{5+} and two V^{4+} ions with partially delocalized 3d electrons. The delocalization of the electrons within each square leads to a large singlet−triplet splitting, with the singlet lying lowest. They are thus not expected to contribute to the magnetic susceptibility at low temperatures. This leaves the four V^{4+} ions at the corners of the large central square in Figure 1a. As shown schematically in Figure 1b they are connected by diarsenite $(As_2O_5)^{4-}$ bridges, which are expected to serve as pathways for weakantiferromagnetic exchange interactions. Numbering the V^{4+} centers as in Figure 1b, we adopt the following spin coupling scheme:

$$\vec{S}_{12} = \vec{S}_1 + \vec{S}_2$$

$$\vec{S}_{123} = \vec{S}_{12} + \vec{S}_3$$

$$\vec{S} = \vec{S}_{123} + \vec{S}_4 \qquad (1)$$

Here $S_i = 1/2$. We are using $|S_{12}S_{123}SM\rangle$ basis functions for our energy and INS intensity calculations. The geometry of the four V^{4+} ions is approximately but not exactly a square. Assuming a Heisenberg interaction with nearest neighbors

(16) Gatteschi, D.; Tsukerblat, B. *Mol. Phys.* **1993**, *79* (1), 121−143.

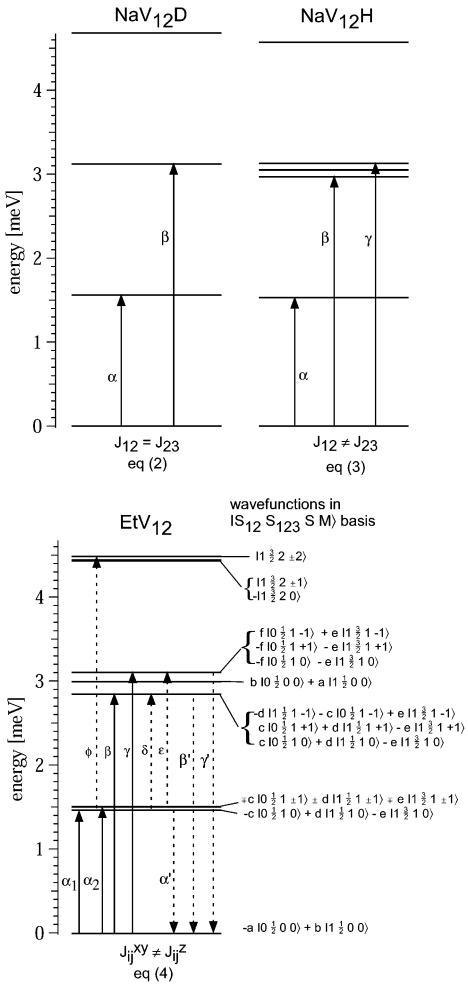

Figure 9. Experimentally determined energy level diagrams for $NaV_{12}H$, $NaV_{12}D$, and EtV_{12}. The allowed cold transitions $\alpha \angle \gamma$ and α_1, α_2 are depicted as full arrows, whereas the dashed arrows belong to hot transitions. The coefficients of the wave functions obtained from a calculation using eq 4 are $a = 0.901$, $b = 0.433$, $c = 0.707$, $d = 0.408$, $e = 0.577$, and $f = 0.816$.

only, we can write the exchange Hamiltonian as

$$\hat{H}_{\text{square}} = -2J(\hat{S}_1\hat{S}_2 + \hat{S}_2\hat{S}_3 + \hat{S}_3\hat{S}_4 + \hat{S}_1\hat{S}_4) \qquad (2)$$

for a square cluster geometry and as

$$\hat{H}_{\text{rectangle}} = -2J_{12}(\hat{S}_1\hat{S}_2 + \hat{S}_3\hat{S}_4) - 2J_{23}(\hat{S}_2\hat{S}_3 + \hat{S}_1\hat{S}_4) \quad (3)$$

for a rectangular geometry.

There is some evidence of anisotropy in the EPR spectrum of some of the cluster levels reported in ref 6. Since our INS data are also indicative of some anisotropy in EtV_{12}, we introduce the following empirical Hamiltonian to account for an axial anisotropy in the rectangular model:

$$\begin{aligned}\hat{H}_{\text{ex}} = -2J_{12}{}^{xy}(\hat{S}_{1x}\hat{S}_{2x} + \hat{S}_{3x}\hat{S}_{4x} + \hat{S}_{1y}\hat{S}_{2y} + \hat{S}_{3y}\hat{S}_{4y}) - \\ 2J_{12}{}^{z}(\hat{S}_{1z}\hat{S}_{2z} + \hat{S}_{3z}\hat{S}_{4z}) - \\ 2J_{23}{}^{xy}(\hat{S}_{2x}\hat{S}_{3x} + \hat{S}_{1x}\hat{S}_{4x} + \hat{S}_{2y}\hat{S}_{3y} + \hat{S}_{1y}\hat{S}_{4y}) - \\ 2J_{23}{}^{z}(\hat{S}_{2z}\hat{S}_{3z} + \hat{S}_{1z}\hat{S}_{4z}) \quad (4)\end{aligned}$$

Energy calculations were carried out in a $|S_{12}S_{123}SM\rangle$ basis using either Hamiltonian (2), (3), or (4) with the program

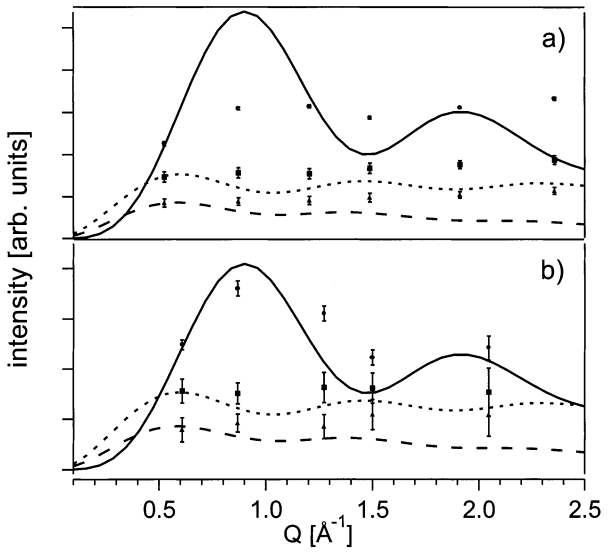

Figure 10. Observed Q dependencies for transitions α (full circles), β (full squares), and γ (full triangles) in the range $Q = 0.1-2.5$ Å^{-1} for compound EtV_{12} (a) in a cylinder and (b) in a slab container. The solid, the fine dotted, and the dotted lines are the calculated Q dependencies for the transitions α, β, and γ, respectively, using eqs 2−4. The calculated curve for transition α was normalized to the experimental intensity at the lowest Q value. The calculated curves for transitions β and γ were normalized to the experimental intensity of transition β at the lowest Q value.

MAGPACK,[17] which is based on the general numerical formalism for solving spin cluster problems developed in ref 18.

The INS intensities are related to the differential neutron cross section. For a transition between the level $|S_{12}S_{123}S\rangle$ at energy E and a level $|S'_{12}S'_{123}S'\rangle$ at energy E' it can be written as[19]

$$\begin{aligned}\frac{\mathrm{d}^2\sigma}{\mathrm{d}\Omega\,\mathrm{d}E} = \left\{\frac{N}{4}\left[\frac{\gamma e^2}{m_e c^2}\right]\frac{|\vec{k}'|}{|\vec{k}|}\exp(-2W(Q,T))\right\}\left\{\sum_{\alpha,\beta}\left\{\delta_{\alpha\beta} - \frac{Q_\alpha Q_\beta}{Q^2}\right\}\sum_{i,j}\{g_i F_i(Q)\}\{g_j F_j(Q)\}\right\}\{\exp(i\vec{Q}(\vec{R}_i - \vec{R}_j))\}\sum_{M,M'}\langle S'_{12}S'_{123}S'M'|\hat{S}^{\alpha}{}_i|S_{12}S_{123}SM\rangle\langle S_{12}S_{123}SM|\hat{S}^{\beta}{}_j| \\ S'_{12}S'_{123}S'M'\rangle\{\delta(\hbar\omega + E - E')\} \quad (5)\end{aligned}$$

In eq 5 $\vec{k}$ and $\vec{k}'$ are the wavevectors of the incoming and scattered neutrons, $\vec{Q} = \vec{k} - \vec{k}'$ is the scattering vector, exp(−2$W(Q, T)$) is the Debye−Waller factor, $\hbar\omega$ is the neutron energy transfer, g_i is the g factor, $F_i(Q)$ is the magnetic form factor of the magnetic ion i, $\vec{R}_i$ is the space vector of the ith vanadium ion in the cluster, α and β stand for the spatial coordinates x, y, and z, e and m_e are the charge and the mass of the electron, respectively, c is the speed of light, and $\gamma = -1.91$ is the gyromagnetic constant of the neutron.

(17) Borrás-Allmenar, J. J.; Clemente, J. J.; Coronado, E.; Tsukerblat, B. S. *J. Comput. Chem.* **2001**, *22* (9), 985.
(18) Borrás-Almenar, J. J.; Clemente-Juan, J. M.; Coronado, E.; Tsukerblat, B. S. *Inorg. Chem.* **1999**, *38*, 6081.
(19) Güdel, H. U.; Hauser, U.; Furrer, A. *Inorg. Chem.* **1979**, *18*, 2730.

Table 5. Comparison of the Exchange Parameters Determined from the Experimental Data[a]

	exchange params (meV)			
compd	J_{12}^{xy}	J_{12}^{z}	J_{23}^{xy}	J_{23}^{z}
$NaV_{12}H$	−0.80	−0.80	−0.72	−0.72
$NaV_{12}D$	−0.78	−0.78	−0.78	−0.78
EtV_{12}	−0.80	−0.82	−0.67	−0.69

[a] Equations 2−4 were used for $NaV_{12}H$, $NaV_{12}D$, and EtV_{12}, respectively.

The following INS selection rules follow directly from eq 5:

$$\Delta S_{12} = \pm 1 \quad \Delta S_{123} = \pm 1$$

$$\Delta S = 0, \pm 1 \quad \Delta M = 0, \pm 1 \tag{6}$$

4.3. INS Data Analysis. The experimentally determined energy level diagrams in Figure 9 were reproduced with the eigenvalues of the Hamiltonians (2)−(4) by varying the exchange parameters. As starting parameters, we used those which were deduced from magnetic and EPR data on the related cluster $[V_{12}As_8O_{40}(HCO_2)]^{5-}$ in ref 6. In $NaV_{12}D$ no splitting of the β/γ transitions is observed, and the position of the β/γ band in Figure 6 is at exactly twice the energy of α. Thus, the most simple Heisenberg Hamiltonian for a square (eq 2) is adequate. It predicts energy levels at exactly $2J$, $4J$, and $6J$. The α INS transition corresponds to the transition at energy $2J$ from the $S = 0$ cluster ground state to the first $S = 1$ excited state. The second excited state at energy $4J$ is triply degenerate, containing two $S = 1$ and one $S = 0$ cluster states. In $NaV_{12}H$ and EtV_{12} β and γ are no longer degenerate, as shown in Figures 6 and 9, and the high-resolution spectra in Figure 8 reveal a clear splitting of α into the two components α_1 and α_2 in EtV_{12}. We therefore used eq 3 to model the splitting in $NaV_{12}H$ and eq 4 for EtV_{12}. In all cases the agreement between experimental and calculated energies is very good, as seen in Table 3. The corresponding exchange parameters are collected in Table 5, and the wave functions for EtV_{12} are given in Figure 9. The wave functions obtained in this energy calculation were then used to calculate the relative intensities of INS transitions as well as their temperature and Q dependence, by applying the formalism introduced in section 4.2. A comparison of experimental and calculated relative intensities for EtV_{12} at various temperatures is given in Table 4. The overall agreement is fair. The important intensity ratio α_1:α_2:β:γ at 1.9 K is well reproduced by the calculation. At higher temperatures the discrepancies are significantly larger. We ascribe this to the larger uncertainties in the experimentalvalues at higher tempertures. Furthermore it is a well-known fact that INS intensities are much more sensitive to small changes of the cluster wave functions than the transition energies. Our wave functions are obviously not perfect, but they are reasonable and lead to very good cluster energies. A very critical ratio is the $\alpha/(\beta + \gamma)$ intensity ratio. In the simple model with a square cluster geometry (eq 2) this ratio is calculated as 2:1, and the experimental value for $NaV_{12}D$ (see Figure 6) is 1.6:1. This is a reasonable agreement.

4.4. Discussion of Exchange Interactions. The exchange splitting patterns determined here for $NaV_{12}H$, $NaV_{12}D$, and EtV_{12} are in good general agreement with the splitting pattern derived from magnetic susceptibility and EPR data of $[V_{12}As_8O_{40}HCO_2]^{5-}$ in ref 6. Using the most simple square model (eq 2) a J value of −0.62 meV was reported in ref 6. Our parameters in Table 5 are more accurate, because they were determined spectroscopically, and we can clearly differentiate between the three compounds, whereas their magnetic properties below 100 K are essentially identical. The differences between the various compounds will be discussed below. But at this point we want to give credit to the authors of refs 6 and 16 for recognizing the important fact that in these $\{V_{12}As_8\}$-type clusters four of the eight unpaired electrons, namely the ones in the outer dark squares in Figure 1a, have no influence on the low-temperature magnetic properties. The large singlet−triplet splitting of the two unpaired electrons within the outer squares is the result of very low lying electron transfer states, which lead to a considerable delocalization and thus spin pairing of these two electrons.

A possible influence of these unpaired electrons becomes apparent when we consider the magnetic behavior at high temperatures. The χT behavior of our three compounds is plotted in Figure 3. Using the exchange parameter values determined by INS for EtV_{12} in Table 5, we computed the magnetic susceptibility as a function of temperature. The result is shown as a full line in Figure 3. The agreement with the experimental data is very good below 100 K. Between 100 and 300 K the experimental data lie above the calculated curve. This is the temperature range in which we also observe differences in the experimental magnetic behavior between the various $\{V_{12}As_8\}$-type clusters. This is seen in Figure 3 and also in a comparison with the published data of $[V_{12}As_8O_{40}(HCO_2)]^{5-}$ in refs 5 and 6. We ascribe these differences and the discrepancy with our calculation to the presence of interactions within the outer squares of these $\{V_{12}As_8\}$-type clusters, which we have neglected and which are different for the various compounds. In all the three compounds studied here the experimental χT values between 100 and 300 K lie above the curve calculated with the INS parameters; see Figure 3. At high temperatures this is due to the population of spin triplet levels arising from the antiferromagnetically coupled electrons in the outer squares.

We therefore attempted to probe this energy region by INS, to localize these higher lying spin levels. The results of our IN4 measurement on the fully deuterated sample $NaV_{12}H$ with 1.1 Å neutrons covering the energy range up to 60 meV, which are shown in Figure 4 in the energy transfer range from 0 to 60 meV, did unfortunately not lead to the desired information. As seen in Figure 4 there are well-defined peaks at 29.3, 34.6, and 48.1 meV and one broad peak centered at around 10 meV. They all show a similar and significant increase of intensity with increasing value of the scattering vector Q. This is a fingerprint of vibrational INS excitations which typically grow in intensity with Q^2. For magnetic excitations we expect a general decrease above 2 $Å^{-1}$

Table 6. Comparison of the Different O−As−O Angles (deg) in the Diarsenite Bridges in Compounds $NaV_{12}H$, $NaV_{12}D$, and EtV_{12}[a]

As(III) ion label		$NaV_{12}H$		$NaV_{12}D$		EtV_{12}	
i	j	δ(O−As_i−O)	δ(O−As_j−O)	δ(O−As_i−O)	δ(O−As_j−O)	δ(O−As_i−O)	δ(O−As_j−O)
A	B	96.65	95.23	96.15	97.06	98.46	98.48
C	D	97.39	96.89	97.06	96.15	97.8	98.03

[a] The numbering scheme refers to the labeling in Figure 1b.

according to the form factor $F(Q)$ in eq 5. We must conclude that any magnetic excitations which might be present in this spectral range are too weak to be detected and characterized, and we are left with the rather indirect argumentation on the basis of the magnetic susceptibility.

Finally we attempt to correlate the differences in the exchange parameters (Table 5) of our three compounds with structural differences within the central V^{4+} square in Figure 1a. As shown in Figure 1b there are two superexchange pathways between adjacent V^{4+} ions through the two ends of the diarsenite bridging ligand. In Table 6 we list the relevant O−As−O angles. We note that for $NaV_{12}D$ all the four angles lie within 1°, in excellent agreement with our finding from the analysis of the INS data that the exchange coupling can be explained with a perfect square model. In $NaV_{12}H$ the variation of the angles is larger, and in particular they are significantly different for the two exchange pathways corresponding to J_{12} and J_{23}. We thus expect the rectangular model (eq 3) to account for the situation, again in agreement with the analysis of the INS results. As seen in Table 5, the two exchange parameters differ by 10%, and this is to be correlated with an average difference of the O−As−O angles of 1.2°. We have no means of determining whether the bigger angle corresponds to the bigger J value or vice versa.

In EtV_{12} the variation of the arsenite angles is not larger than in $NaV_{12}D$, and yet J_{12} and J_{23} are significantly different; in addition, we had to use the anisotropic Hamiltonian (eq 4) to account for the splitting of the α transition into the two lines α_1 and α_2. The $\{V_{12}As_8\}$-type cluster in EtV_{12} does not lie on a center of inversion. One V═O bond within one outer square is pointing toward the center of the $\{V_{12}As_8\}$-type cage, as shown in Figure 2 (strong bond), whereas all the other eleven V═O double bonds are pointing away from the cluster. In addition, the corresponding vanadium ion is also moved slightly to the center of the cluster so that this outer square is strongly distorted; see Figure 1a. The crystal structure of EtV_{12} contains only a single species (see above), in contrast to the structures of $NaV_{12}H$ and $NaV_{12}D$. The disorder of these latter structures is related to the in/out isomerism of the V═O double bond described above for EtV_{12}. In both $NaV_{12}H$ and $NaV_{12}D$ both positions can be occupied, leading to a formation of different species. A direct result of this disorder can be seen in Figure 8, where the α peak is inhomogeneously broadened, in contrast to EtV_{12}, where α_1 and α_2 are resolved. We conclude that the α transition is also split in the $NaV_{12}H$ and $NaV_{12}D$ samples, but it cannot be resolved as a result of the structural disorder. We model the α_1/α_2 splitting in EtV_{12} with the empirical exchange Hamiltonian using eq 4. This does not tell us anything about the physical origin of the deviation from the isotropic model. It could be true anisotropic in origin or it could be antisymmetric exchange.

4.5. INS on Deuterated and Nondeuterated Samples. The principal limiting factors for a wide application of INS in the area of spin clusters are the following: (1) A relatively large amount (at least 3−5 g of polycrystalline material) is needed for the experiments. (2) The presence of hydrogen atoms in the sample may adversely affect the observation of magnetic cluster excitations due to strong incoherent nuclear scattering by hydrogen atoms.

Our experimental results collected for the three samples $NaV_{12}H$, $NaV_{12}D$, and EtV_{12}, all containing the same $\{V_{12}As_8\}$-type cluster, allow us to draw some conclusions concerning point 2. Figure 5 compares survey INS spectra of $NaV_{12}H$, $NaV_{12}D$, and EtV_{12} measured with low instrumental resolution at 1.5 K. Whereas $NaV_{12}H$ only contains H_2O molecules, the EtV_{12} sample is more typical of the majority of spin clusters in that it contains organic groups, in the present case the $(Et_3NH)^+$ cation. As seen in Figure 5, the EtV_{12} sample shows intense inelastic features above 5 meV which are absent in the other spectra. While an assignment of individual features to specific internal or external molecular vibrations cannot be made on the basis of the existing data, it is nevertheless clear that the scattering in this spectral range is due to vibrations in which hydrogen atoms with their large incoherent cross section are involved. Below 5 meV there is a general contribution of incoherent scattering for both $NaV_{12}H$ and EtV_{12} to the background. But this does not preclude the measurement of magnetic inelastic excitations, as illustrated in Figures 6−8. So we have a spectral window, from about 0.2 meV (depending on the instrumental resolution) to about 5 meV, which is also accessible for the measurement of magnetic excitations in nondeuterated samples of molecular spin clusters. Recent measurements of anisotropy splitting by INS in the Fe_8 [14] Mn_{12} [11] clusters and a series of Mn_4 clusters,[15] all containing hydrogen atoms, were all performed in this spectral range. This does not mean that magnetic excitations in this spectral range can be measured in any sample containing hydrogen. We have experienced several failures in recent years using undeuterated samples, where the background was too high to detect magnetic excitations even between 0.2 and 5 meV. For each chemical composition the competition between coherent and incoherent scattering as well as absorption has to be evaluated separately.

A typical result of the presence of H atoms is shown in Figure 10a, where the measured Q dependences of the α, β, and γ bands in energy loss at 1.9 K of a EtV_{12} sample in a cylindrical container of 15 mm diameter are plotted. The experimental data do not correspond to the theoretically

expected *Q* dependence for these magnetic excitations; see the lines in Figure 10. The *Q* dependence is essentially washed out. Figure 10b shows the same comparison for a sample of EtV_{12} as described above but in a slab container of 2 mm thickness. There is a *Q* dependence in the experimental data, in particular for the α transition, and it approaches the calculated one. We have made very similar observations with other spin cluster samples containing hydrogen atoms, and we explain it as follows. In a thick sample, e.g. a cylinder of 15 mm diameter, each neutron undergoing a magnetic INS process of the spin cluster is suffering several incoherent elastic scattering processes from H atoms when crossing the sample. As a result, it will lose its well defined wavevector and the *Q* dependence of the magnetic transition will be washed out. By using a thin sample, e.g. a slab of 2 mm sample thickness, this problem is greatly reduced due to the reduced number of incoherent processes from H atoms that each neutron is suffering, as illustrated in Figure 10b. There is important information in the *Q* dependence about the nature of the magnetic cluster excitations and thus, indirectly, about the cluster wave functions. We conclude that slab containers must be used in INS studies of undeuterated spin clusters, if at least part of this information is to be retrieved.

5. Conclusions

By using inelastic neutron scattering on a series of related $\{V_{12}As_8\}$-type cluster compounds, we confirm the essential correctness of an earlier model developed on the basis of magnetic and EPR measurements. The exchange parameters could be derived very accurately since INS provides direct access to the exchange splittings. This allows a rather detailed correlation with the structure of the relevant cluster, in particular the O−As−O angles of the diarsenite bridges between the V^{4+} ions. In EtV_{12}, the first excited triplet level is split by 0.05 meV which is the result of either anisotropic or antisymmetric exchange. The present study of the same $\{V_{12}As_8\}$-type cluster in three different crystal environments allows us to draw some conclusions concerning the applicability of INS in the area of undeuterated molecular spin clusters. For favorable chemical compositions it is possible to measure magnetic excitations with reasonable statistics in the spectral range 0.2−5 meV. To extract the important dependence of the cross section on the scattering vector *Q*, it is important to use slab containers whenever the sample contains H atoms.

Acknowledgment. R.B. thanks Prof. Thomas Armbruster for his support in characterizing the samples. This work was financially supported by the Swiss National Science Foundation (Grant NFP-47) and the European Union under Contract HPRN-CT-1999-00012. A.M. acknowledges financial support from the Deutsche Forschungsgemeinschaft and the Fonds der Chemischen Industrie.

Supporting Information Available: Two X-ray crystallographic files, in CIF format, are available. This material is available free of charge via the Internet at http://pubs.acs.org.

IC0202099